Colloids and Surfaces B: Biointerfaces 71 (2009) 160–167

Contents lists available at ScienceDirect

Colloids and Surfaces B: Biointerfaces

journal homepage: www.elsevier.com/locate/colsurfb

Escherichia coli transport in porous media: Influence of cell strain, solution chemistry, and temperature

Hyunjung N. Kim, Sharon L. Walker*

Department of Chemical & Environmental Engineering, University of California, Riverside, CA 92521, United States

ARTICLE INFO

Article history:
Received 2 May 2008
Received in revised form 11 December 2008
Accepted 3 February 2009
Available online 11 February 2009

Keywords:
Bacterial deposition
E. coli
Temperature
Valence
Packed bed

ABSTRACT

Packed bed column and complementary characterization experiments were carried out with two *Escherichia coli* strains (D21g and XL1-Blue) under a range of ionic strength (IS) and valence (KCl, $CaCl_2$, and artificial groundwater) to determine the role of bacterial strain and solution chemistry on cell adhesion. Increasing IS and valence had a marked effect on the electrokinetic and surface properties of bacteria and quartz grains; hence resulting in a greater rate of deposition. Distinct deposition trends were observed for the two cell strains, with greater retention observed for D21g versus XL1-Blue across the range of IS. Selected transport and characterization experiments were also conducted with the D21g cells, finding deposition also increasing with IS and valence. In the presence of Ca^{2+} bacterial deposition behavior deviated from anticipated trends and it is concluded from additional analysis that Ca^{2+} ions influence bacterial surface charge, hydrophobicity, and extracellular polymers. Further transport experiments were conducted with the D21g cells and colloids to establish the role of temperature (4, 10 and 25 °C). Results suggested that a combination of specific and non-specific interactions occurring between the cells and quartz determines the extent of deposition, rather than transport from the bulk to the collector surface.
© 2009 Elsevier B.V. All rights reserved.

1. Introduction

The fate and transport of microorganisms in the subsurface environment has been a subject of considerable interest for natural and engineered systems [1,2]. Hence, a complete understanding of the mechanisms controlling bacterial fate in porous media is essential to protect our water resources. Consequently, research has been conducted to investigate key physical, chemical and biological factors influencing bacterial transport including physical parameters such as porous media [3], temperature [4], and fluid velocity [5]; chemical factors including ionic strength (IS) and valence [6] and pH [7]; and biological factors such as cell type [8], hydrophobicity [9], surface charge of the bacteria [10], and bacterial concentration [11]. Among these, physical and chemical factors have been investigated most extensively [3,12,13] and considerably less is known of biological factors. It has been observed that bacterial surface polymers including lipopolysaccharides (LPS) [14] and extracellular polymeric substances (EPS) [15] are very sensitive to solution chemistry [6,16] and environmental stress [14,17]. However, due to the complexity of bacteria it is evident that these biological conditions must be investigated further.

The majority of previous work has been conducted at room temperature [3,5,6] due to the misconception that temperature impacts bacterial transport less significantly than other factors. Recently, Castro and Tufenkji [18] found temperature impacts transport of a pathogenic *Escherichia coli*; however, they observed this sensitivity did not exist for the non-pathogenic strains tested. McCaulou et al. [4] also observed the role of temperature, with motile bacterial retention notably greater at a lower temperature (4 °C versus 18 °C) as opposed to colloid filtration theory [19] which predicts only minor sensitivity of travel distance to temperature [20]. However, the actual temperature of groundwater is approximately 10 °C [21] and this varies seasonally [22]. Therefore assuming that room temperature experimentation allows for approximation of bacterial transport in groundwater environments may not be valid [18].

Although it has been shown that solution chemistry [6,16] and temperature [4,18] played a role in bacterial adhesion, few have focused on the coupled role of these factors. Thus, the objective of this study was to systematically investigate the physical, chemical, and biological phenomena influencing cell transport through study of the role of bacterial strain, solution chemistry, and temperature utilizing packed bed column experiments and extensive cell characterization. For this purpose, two *E. coli* strains (D21g and XL1-Blue) were selected to examine the influence of cell strain, and the transport experiments were performed with mono-, di-, and multivalent ions and at 4, 10, and 25 °C to establish the role of valence and temperature. Furthermore, the extent to which the deposition trends

* Corresponding author. Tel.: +1 951 827 6094; fax: +1 951 827 5696.
E-mail address: swalker@engr.ucr.edu (S.L. Walker).

0927-7765/$ – see front matter © 2009 Elsevier B.V. All rights reserved.
doi:10.1016/j.colsurfb.2009.02.002

were biological phenomena, parallel experiments were conducted using a model colloid for comparison.

2. Materials and methods

2.1. Bacterial and colloid selection

E. coli D21g [23] and *E. coli* XL1-Blue (Stratagene, La Jolla, CA) [24], both non-flagellated K-12 strains, were used. A cell suspension of $(1–5) \times 10^7$ cells mL^{-1} was used for transport experiments. 1.0 μm surfactant-free carboxylate modified latex (CML) particles with a density 1.055 g cm^{-3} at 25 °C (Interfacial Dynamics, Portland, OR) were used as a model particle to compare with bacteria. The particle concentration utilized for experiments was $(1–5) \times 10^7$ particles mL^{-1}.

2.2. Bacterial preparation and growth

E. coli D21g and XL1-Blue cells were grown in Luria–Bertani Broth (Fisher Scientific, Fair Lawn, NJ) at 37 °C in the presence of 0.03 g L^{-1} gentamicin (Sigma, St. Louis, MO). All cultures were harvested at mid-exponential phase by centrifugation (Fisher accuSpin* 3R Centrifuge, Fisher Scientific) for 15 min at $3689 \times g$ (Swing Bucket Rotor 7500, Fisher Scientific). The cells were rinsed two additional times using a 10 mM KCl or $CaCl_2$, based upon the solution chemistry of the subsequent experiment, to remove any remaining growth media. The cells were re-suspended in 5 mL of the electrolyte and this solution was used to determine cell concentration in a counting chamber (Marienfeld Laboratory Glassware, Lauda-Kőenigshofen, Germany).

2.3. Solution chemistry

In order to investigate the effect of valence, KCl (Fisher Scientific) and $CaCl_2$ (Fisher Scientific) were selected as electrolytes. The IS ranges utilized in transport experiments were 3–300 mM KCl and 3–150 mM $CaCl_2$. The pH was unadjusted (5.6–5.8). Additionally, to compare these simple electrolytes with a groundwater environment, artificial groundwater (AGW) was utilized in a few representative transport experiments. 10 mM AGW was composed of 0.014 g KNO_3, 0.321 g $MgSO_4 \cdot 7H_2O$, 0.112 g $CaSO_4 \cdot 2H_2O$, 0.044 g NaCl, and 0.109 g $NaHCO_3$ per 1 L of deionized water [25]. Prior to the experiment, AGW was filtered with 0.22 μm filter (Millipore, Billerica, MA) to ensure sterility. The measured pH of AGW was approximately 8.0.

2.4. Bacterial and particle characterization

Viability tests were conducted for the bacteria suspended in 10 mM KCl, $CaCl_2$, and AGW. Cells were stained using the Live/Dead® BacLight™ kit (L-7012, Molecular Probes, Eugene, OR) and observed with an inverted fluorescent microscope (IX70, Olympus, Japan) using a red/green fluorescence filter set (Chroma Technology Corp., Brattleboro, VT). The reported viability is the percentage of all cells which remained viable under each condition.

To evaluate the size of the cells, images of the cells were taken with an inverted microscope (IX70, Olympus, Japan) in phase contrast mode. From these images, the lengths and the widths of the cells ($n \geq 50$) were automatically measured by an image processing program (SimplePCI, Precision Instruments, Inc., Minneapolis, MN) and the equivalent radii of the cells calculated.

The electrophoretic mobility of the bacteria were evaluated at 25 °C as a function of IS in the presence of KCl and $CaCl_2$ using a ZetaPALS analyzer (Brookhaven Instruments Corporation, Holtsville, NY). For D21g cells, the electrophoretic mobility was also measured in 10 mM AGW (25 °C). Furthermore, the electrokinetic properties of D21g and colloids were analyzed in triplicate at all experimental temperatures and IS in KCl and $CaCl_2$. However, the lowest temperature tested was 6 °C due to the lower limit of the ZetaPALS equipment. Electrophoretic mobility was converted to zeta potential using the Smoluchowski equation [20].

The hydrophobicity of colloids and bacteria was measured by the microbial adhesion to hydrocarbons (MATH) test [26]. 1 mL of *n*-dodecane (laboratory grade, Fisher Scientific) was added to 4 mL of a particle suspension, and the mixture was vortexed (AutoTouch Mixer Model 231, Fisher Scientific). After leaving the sample for 45 min, the optical density of the water phase was measured at 546 nm. The percentage of particles partitioned to oil phase was calculated [26].

In order to further compare the two *E. coli* strains, potentiometric titration was conducted using a microtitrator (798 Titrino, Metroohm, Switzerland). Samples were purged with N_2 gas (Puritan Medical Products, Inc., Overland Park, KS) prior to experiments. The relative acidity and surface charge density were calculated from the amount of NaOH consumed when titrating the bacterial suspension between pH 4 and 10 [27].

The EPS content and composition (protein and polysaccharides) were analyzed. The EPS was extracted from the bacterial cells based upon a previously established method [6]. Once extracted, the proteinaceous content of the extracellular material was analyzed by the Lowry method [28] whereby the protein content was determined spectroscopically (BioSpec-mini, Shimadzu Corp., Kyoto, Japan) at a wavelength of 500 nm, and calibrated with bovine serum albumin (BSA, 20 mg mL^{-1}) (Fisher BioReagents, Fisher Scientific). Total polysaccharide content was analyzed using the phenol–sulfuric acid method [29], measured spectroscopically (488 nm), and using Xanthan gum (Sigma–Aldrich, St. Louis, MO) as the standard.

To investigate the influence of temperature on the cell and particle properties, samples were harvested, suspended in the background electrolyte, incubated for an hour at the desired temperature in a water bath (Transsonic 460/H, Barnstead/Lab-line, IL, USA), and then immediately analyzed by the procedures described above or used it for transport experiments.

2.5. Column experiments and porous media

Ultra-pure quartz sand (Iota® quartz, Unimin Corp., NC) was used as the packing material for the column experiments. The sand was sieved between 250 and 300 μm U.S. standard stainless steel test sieves (Fisher Scientific) such that the average sand diameter (d_{50}) was 275 μm. To remove any metal and organic impurities, the sand was thoroughly cleaned [23]. Prior to wet-packing the column, the cleaned sand was re-hydrated by a boiling in deionized water for 1 h. The bed porosity was measured gravimetrically and averaged 0.46. For favorable (i.e., non-repulsive) transport experiments the sand surface was treated with a 1% (v/v) solution of 3-aminopropyl-triethoxysilane (Sigma–Aldrich, St. Louis, MO) by a previously published method [30]. The favorable experiments were conducted in 10 mM solution.

An adjustable length chromatography column (Omnifit, Boonton, NJ) with a 1.5 cm inner diameter was used for transport experiments. The column length was adjusted (3.5–11.2 cm) to ensure a measurable effluent concentration. Ten pore volumes (PVs) of deionized water were pumped through the column by a syringe pump (KD Scientific Inc., New Hope, PA) followed by 5–6 PVs of the desired electrolyte to equilibrate the column. Four PVs of the bacteria or colloid suspension was injected followed by a particle free electrolyte solution (6 PVs). The superficial velocity was maintained at 0.017 cm s^{-1} for all experiments. Calculated Reynolds number and Peclet number values for the packed bed was 0.1 and 0.2, respectively [20]. The effluent concentration was measured at 280 nm by a UV/Vis spectrophotometer (SP-890, Barnstead Interna-

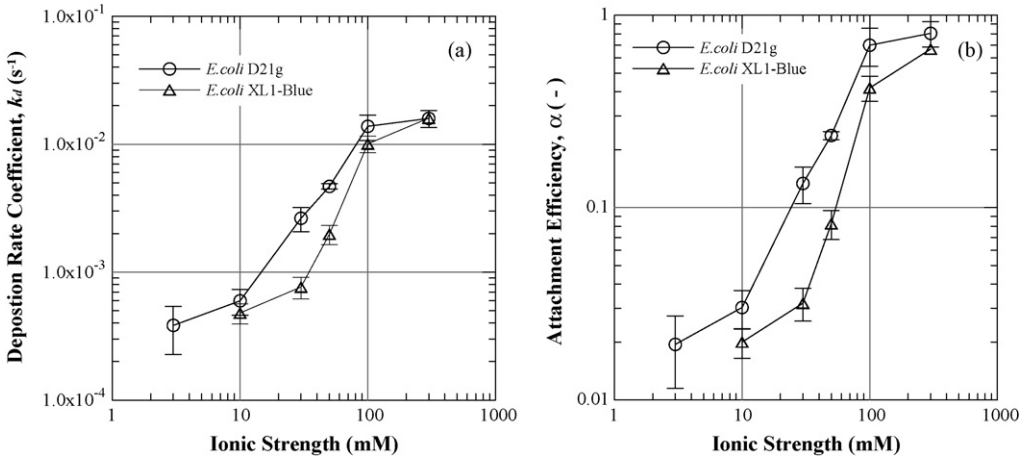


Fig. 1. Comparison of *E. coli* D21g and XL1-Blue transport. (a) Deposition rate coefficients (k_d) and (b) attachment efficiency (α) for D21g and XL1-Blue as a function of IS. Experiments were performed with KCl and at 25 °C. Error bars indicate one standard deviation.

tional, Dubuque, IA). The column experiments at low temperature (4 and 10 °C) were conducted in a cold room. Experiments at high temperature (25 °C) were conducted in the ambient air of the laboratory. For experiments conducted at 25 °C, a micro-flow-through cuvette (Fisher Scientific) was used; however, a fraction collector (CF-1 Fraction Collector, Spectrum® Chromatography, Houston, TX) was used for 4 and 10 °C experiments as the spectrophotometer could not operate at the lower temperatures.

2.6. Quantifying extent of deposition

In order to compare the deposition kinetics of bacteria and colloids, the deposition rate coefficient, k_d (s^{-1}), was determined by [31]:

$$k_d = -\frac{U}{\varepsilon L} \ln\left[\frac{C}{C_0}\right] \quad (1)$$

where C/C_0 is the "clean bed" concentration exiting the column (obtained between 1.8 and 2.0 PV [32]), U is superficial velocity, ε is porosity, and L is length of the packed bed. An experimentally determined attachment efficiency (α) was obtained by [31]:

$$\alpha = \frac{k_d}{k_{d,fav}} \quad (2)$$

where k_d and $k_{d,fav}$ are deposition rate coefficients as determined for unfavorable and favorable conditions, respectively.

In order to predict the sensitivity of D21g cells and CML particles to temperature, single collector efficiency (η_0) was calculated from the relationship developed by Tufenkji and Elimelech [33]. For these calculations values of 275 μm and 1.05 g cm^{-3} (1.055 g cm^{-3}) were input as the average diameter of a collector and the density of the cell/colloid, respectively. Values of 6.5×10^{-21} J [23] and 1.0×10^{-20} J [34] were utilized for the Hamaker constant of bacteria and colloids.

3. Results and discussion

3.1. Effect of cell strain on bacterial deposition

The experimentally determined values of deposition rate (k_d) and attachment efficiency (α) for *E. coli* D21g and XL1-Blue cells are shown in Fig. 1a and b, respectively. The average k_d and α of D21g cells were consistently greater than those of XL1-Blue over the range of IS (10–100 mM), with a maximum difference occurring at 30 mM. For D21g, the k_d ranged from 3.8×10^{-4} to 1.6×10^{-2} s^{-1} and α values varied from 0.02 to 0.8 across the same range of IS. For XL1-Blue, the average k_d and α were distributed from 4.8×10^{-4} to 1.6×10^{-2} s^{-1} and from 0.02 to 0.67, respectively. Overall, k_d and α values for both strains increased with IS until reaching a plateau, indicating that above this IS there exists a transport-limited regime with no electrostatic energy barrier between the bacteria and quartz grains [23]. For D21g, k_d and α increased up to 100 mM, while XL1-Blue deposition rate and attachment efficiency showed sensitivity to IS up to 300 mM. These trends result from electrical double layer compression occurring at high IS, as captured by the classic Derjaguin–Landau–Verwey–Overbeek (DLVO) theory [35]. As noted in Table 1, the favorable deposition rate coefficients ($k_{d,fav}$) of D21g and XL1-Blue were experimentally determined to be 2.0×10^{-2} and 2.4×10^{-2} s^{-1}, respectively.

At room temperature, *E. coli* D21g and XL1-Blue cells were characterized (Table 1) and the equivalent diameters were quite similar at 0.96 and 1.1 μm, respectively. The viability of D21g (90.1%) and XL1-Blue (90.9%) was also measured. Zeta potential values were also determined (Fig. 2), and it was observed cells become less negatively charged with increasing IS. This is consistent with the deposition trends for both strains, where the zeta potential of XL1-Blue was not only more negative than that of D21g – up to 100 mM IS with maximum difference at 30 mM IS – it was also less adhesive as shown by lower k_d and α values (Fig. 1). These results suggest electrostatic forces are a dominate interaction mechanism under the conditions investigated in this study.

The hydrophobicity of XL1-Blue (54%) was considerably greater than that of D21g (21%). These results did not correspond with the bacterial deposition behavior, suggesting hydrophobic interaction between cells and quartz surfaces was not the mechanism controlling cell deposition.

Potentiometric titration (Table 1) indicated that D21g cells have more polar functional groups than XL1-Blue exposed on the outer membrane surfaces and within the extracellular polymeric matrix. Additionally, the shapes of the titration curves obtained for both cells were similar (graphs not shown), indicating that the two *E. coli* strains have the same exposed of functional groups [27,36]. This is consistent with other measurements, in that D21g with higher acidity and surface charge density also was found to be more hydrophilic.

It has been reported that *E. coli* strains used in this study typically produces very small amounts of EPS [36–38] which agrees with our experimental results (Table 2). The two *E. coli* strains had roughly the same order of magnitude and low levels of EPS content with D21g and XL1-Blue having 52.8 mg and 71.8 mg EPS per 10^{10} cells, respectively. D21g had greater amount of protein than XL1-Blue; while the polysaccharide level was almost identical. The ratio of

Table 1
Transport and surface characteristics of *E. coli* D21g and XL1-Blue. Ionic strength of all electrolytes presented here is 10 mM.

Cell type	Temperature (°C)	Radius (μm)[a]	Zeta potential (mV)	Acidity (mequiv./10^8 cell)[b]	Surface charge density (μC cm^{-2})[c]	MATH (%)[d]	Live (%)[e]	k_d (s^{-1})[f]	$k_{d,fav}$ (s^{-1})	η_0
D21g in KCl	4	0.48	−46.8 ± 3.2	ND[g]	ND	ND	90.3 ± 2.3	$8.1 \times 10^{-4} \pm 2.4 \times 10^{-4}$	$2.3 \times 10^{-2} \pm 1.2 \times 10^{-3}$	2.6×10^{-3}
	10	0.50	−50.9 ± 0.7	ND	ND	ND	90.1 ± 0.7	$1.4 \times 10^{-3} \pm 2.2 \times 10^{-4}$	$2.0 \times 10^{-2} \pm 3.5 \times 10^{-3}$	2.9×10^{-3}
	25	0.48	−56.8 ± 2.5	8.7×10^{-5}	2930	21.5 ± 0.8	90.1 ± 0.7	$6.0 \times 10^{-4} \pm 1.4 \times 10^{-4}$	$2.0 \times 10^{-2} \pm 1.8 \times 10^{-3}$	3.8×10^{-3}
XL1-Blue in KCl	25	0.55	−60.1 ± 2.6	1.7×10^{-5}	439	54.4 ± 3.3	90.9 ± 2.2	$4.8 \times 10^{-4} \pm 8.5 \times 10^{-5}$	$2.4 \times 10^{-2} \pm 8.1 \times 10^{-4}$	ND
D21g in $CaCl_2$	4	ND	−20.1 ± 2.1	ND	ND	ND	ND	$2.0 \times 10^{-3} \pm 5.1 \times 10^{-4}$	$2.7 \times 10^{-2} \pm 5.3 \times 10^{-4}$	2.6×10^{-3}
	10	ND	−21.3 ± 2.9	ND	ND	ND	ND	$2.7 \times 10^{-3} \pm 5.0 \times 10^{-4}$	$2.3 \times 10^{-2} \pm 1.9 \times 10^{-3}$	2.9×10^{-3}
	25	ND	−20.8 ± 1.7	ND	ND	55.1 ± 2.3	95.8 ± 0.2	$2.3 \times 10^{-3} \pm 7.7 \times 10^{-4}$	$2.3 \times 10^{-2} \pm 1.3 \times 10^{-3}$	3.8×10^{-3}
D21g in AGW	25	ND	−31.2 ± 2.7	ND	ND	11.9 ± 1.5	95.7 ± 0.9	$1.2 \times 10^{-3} \pm 5.3 \times 10^{-4}$	$1.2 \times 10^{-2} \pm 1.0 \times 10^{-3}$	ND

[a] Value for equivalent spherical radius calculated from experimentally measured length and width of individual cells.
[b] Acidity determined from the amount of NaOH consumed during a titration between pH 4 and 10 for cells suspended in 10 mM KCl.
[c] Indicates the density of charged functional groups across the cell surface. Value determined from the experimentally measured acidity, and accounting for the exposed surface area of the cells (calculated for a spherical cell) and Faraday's constant of 96,485 C mol^{-1}.
[d] Microbial adhesion to hydrocarbon (MATH) indicates the relative hydrophobicity of the cell as the percent of cells partitioned in dodecane versus electrolyte (10 mM KCl or 3.33 mM $CaCl_2$ as molar concentration).
[e] Percent of cell population determined to be viable based on the Live/Dead BacLight® kit at 10 mM KCl or 3.33 mM $CaCl_2$ (as molar concentration).
[f] Data are same as Figs. 1 and 3.
[g] Not determined.

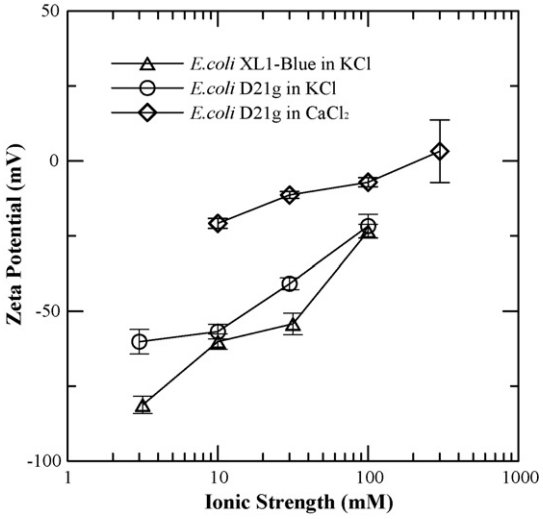


Fig. 2. Zeta potential for *E. coli* D21g and XL1-Blue. All experiments were performed at 25 °C. Error bars indicate one standard deviation.

sugar to protein (SP ratio) was found to be up to 5 times greater for XL1-Blue than D21g.

On the basis of the cell and EPS characterization for two strains, the deposition behavior of the D21g and XL1-Blue can be explained as follows. As the *E. coli* strains were found to have negligible amounts of EPS, these polymers may not fully cover the bacterial surface. This leaves the LPS and proteins onto the outer membrane partially exposed and capable of influencing the charged nature of the cells. Consequently, the exposed outer membrane structures may enhance the hydrophobicity of XL1-Blue, and contribute to the XL1-Blue having a higher electrophoretic mobility than D21g. Additionally, the higher relative protein content in the D21g EPS may lead to greater electrostatic attraction between the cells and quartz surface, as compared to the XL1-Blue on which the greater SP ratio contributes to the hydrophobic nature.

3.2. Influence of valence

Average k_d values for D21g in the presence of two simple electrolytes, KCl and $CaCl_2$, at room temperature (25 °C) are presented in Table 1. The k_d value of D21g in the presence of $CaCl_2$ (2.3×10^{-3} s^{-1}) is approximately four times greater than in KCl (6.0×10^{-4} s^{-1}). Also, the k_d and α values in the presence of either electrolyte increase with IS, and reach plateau at 100 mM (Figs. 3 and 4). In KCl, k_d values ranged from 3.8×10^{-4} to 1.6×10^{-2} s^{-1}, and α from 0.02 to 0.8. In $CaCl_2$, k_d and α values extended from 1.1×10^{-3} to 3.0×10^{-2} s^{-1}, and from 0.05 to 1.33, respectively. Overall, the k_d and α values of D21g in $CaCl_2$ were substantially greater than those in KCl over the IS investigated; and interestingly, the trend was continuous even at higher IS conditions where no energy barrier to deposition should exist. Furthermore, the $k_{d,fav}$ of D21g in the presence of $CaCl_2$ is slightly greater than in KCl with a confidence level of 95% ($P < 0.05$).

Zeta potential of D21g in KCl or $CaCl_2$ is sensitive to IS (Fig. 2). Over the entire range of IS investigated zeta potential values in $CaCl_2$ were much less negative than in KCl. The reduction in zeta potential with increasing electrolyte concentration and valence is attributed to double-layer compression [39]. Furthermore, hydrophobicity data (Table 1) indicated that cells in $CaCl_2$ are more hydrophobic than those in KCl (approximately 55% and 21%, respectively).

Transport experimental results indicate that divalent ions (Ca^{2+}) substantially enhance D21g k_d and α values as compared with the monovalent ion (K^+). Results are well supported by the measured

Table 2
EPS composition for *E. coli* D21g and XL1-Blue.

Cell type	Method	Temperature (°C)	EPS (mg/10^{10} cells)	Sugar (μg/10^{10} cells)[a]	Protein (μg/10^{10} cells)[b]	Sugar/protein ratio
D21g	Ethanol	4	66.3 ± 4.1	90.6 ± 12.2	1465 ± 129	0.06
		10	57.8 ± 3.6	85.1 ± 11.1	1411 ± 112	0.06
		25	52.8 ± 2.5	73.9 ± 8.0	1134 ± 257	0.07
XL1-Blue	Ethanol	25	71.8 ± 6.5	64.9 ± 49.7	177 ± 30	0.37

[a] Based on Xanthan gum as the standard.
[b] Based on bovine serum albumin (BSA) as the standard.

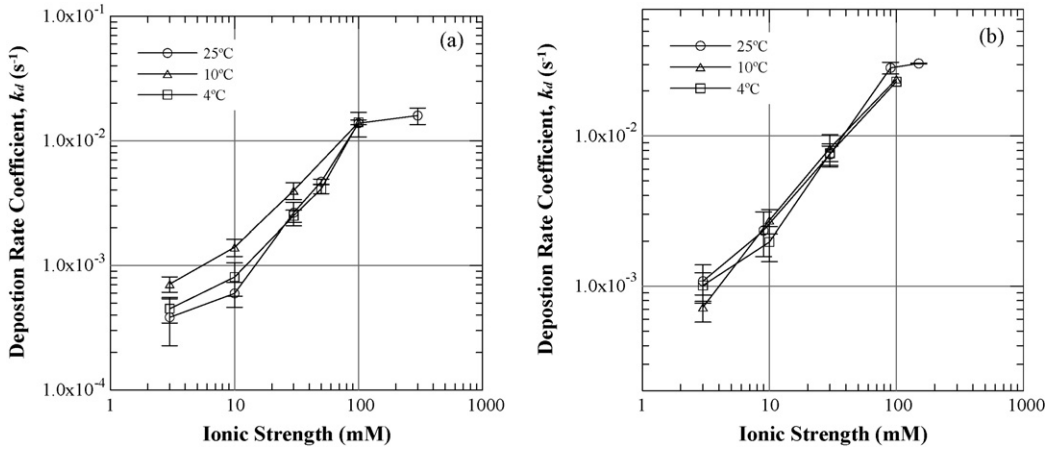


Fig. 3. Deposition rate coefficients (k_d) for *E. coli* D21g in the presence of (a) KCl and (b) $CaCl_2$ as a function of temperature. Data for D21g at 25 °C in KCl are same as Fig. 1. Error bars indicate one standard deviation.

electrokinetic properties of D21g, with the more negatively charged cells having lower k_d and α values than cells in $CaCl_2$. Furthermore, the increased hydrophobicity of the cells in the presence of Ca^{2+} may contribute to the greater attachment as compared with K^+ [40,41]. Previously divalent cation bridging (DCB) theory [42,43] was proposed to explain the role of divalent cations on aggregation and stabilization of microbial polymers, suggesting that Ca^{2+} causes non-specific interactions with negatively charged functional groups distributed in the EPS and on the cell outer membrane. Therefore, differences in zeta potential and relative hydrophobicity between D21g in KCl and $CaCl_2$ may be attributed to this mechanism. Additionally recent work has credited Ca^{2+} with charge neutralization and subsequent re-conformation of bacterial polymer structure [6,16,40]; Ca^{2+} has also been observed to contribute to an attractive force between colloid and membrane surfaces through atomic force microscopy (AFM) [44]. The combination of these mechanisms leads to decreased zeta potential, increased hydrophobicity, and ultimately enhanced cell interactions with the surface.

Classic DLVO theory suggests that α values should approach unity under mass transport-limited conditions when the energy barrier is overcome [20,23]; however, these experimental results are not consistent with this. Specifically, α values for D21g in the presence of $CaCl_2$ at high IS are greater than unity (Fig. 4b). This may be attributed to greater concentrations of $CaCl_2$ enhancing bridging with the negatively-charged functional groups exposed on the cells, further contributing to cell-quartz interactions under higher IS conditions. This bridging phenomena, or enhanced interactions, was recently observed in a radial stagnation point flow chamber [6,16], multi-angle light scattering system [39], and AFM [44].

In order to investigate the deposition behavior of D21g in a multi-valent solution, AGW was utilized. The experimental results obtained at unfavorable and favorable conditions in AGW are shown

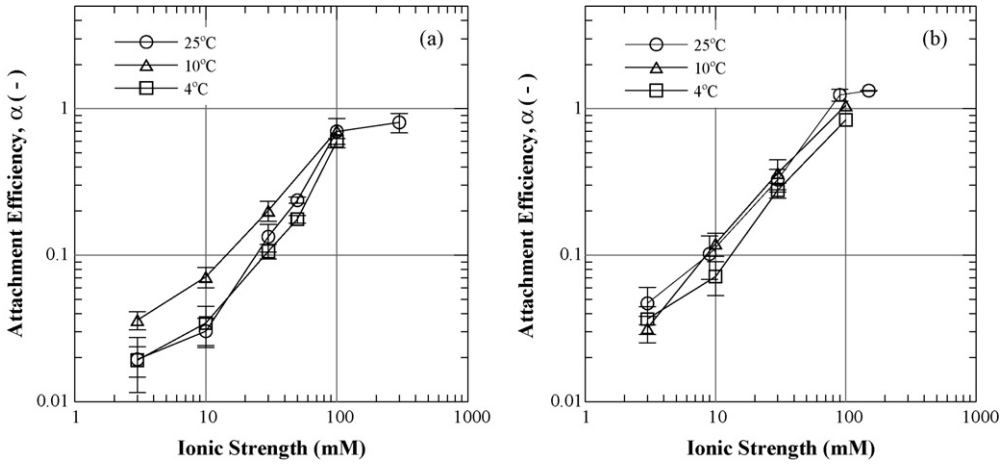


Fig. 4. Attachment efficiency (α) for *E. coli* D21g in the presence of (a) KCl and (b) $CaCl_2$ as a function of temperature. Error bars indicate one standard deviation.

in Table 1, respectively. The k_d value in the presence of AGW was between those obtained for KCl and $CaCl_2$ solutions (Table 1). Although the pH and composition of AGW differs from the other simple electrolytes, deposition trends can still be explained by electrostatic interactions between D21g and quartz. Specifically, the zeta potential of D21g in AGW was more negative than in $CaCl_2$ (Table 1), but less than when suspended in KCl—similar to the deposition trends. Results suggest that the unfavorable deposition trends for D21g in K^+ and Ca^{2+} captures the behavior of cells as would occur in a multi-valent electrolyte.

The $k_{d,fav}$ value in the presence of AGW was determined to be 1.2×10^{-2} s^{-1} and around two times lower than those in KCl or $CaCl_2$ solution. This behavior is attributed to the change of the surface potential of the silanized quartz (−14 mV in 10 mM AGW at pH 8). As the silanized quartz is negatively charged at pH 8, there is a reduced electrostatic attraction experienced between the cells and modified quartz as compared to the lower pH (5.6–5.8) conditions, resulting in a lower transfer rate.

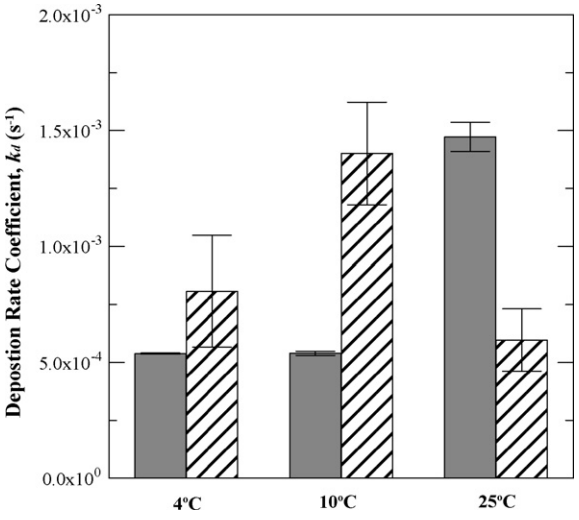


Fig. 5. Deposition rate coefficients (k_d) for CML particles (solid) and D21g (shade) in the presence of 10 mM KCl as a function of temperature. Data for D21g are same as Fig. 3a. Error bars indicate one standard deviation.

3.3. Influence of temperature

In this study, the relative significance of physicochemical and biological factors that accompany temperature changes have been examined and results demonstrate that temperature does not cause a major difference in cell transport and surprisingly, deposition behavior of D21g cells differed from inert CML colloids.

Average k_d and α values of D21g as a function of temperature in the presence of KCl are presented in Figs. 3a and 4a. Regardless of temperature, k_d and α values increased with IS and data converges around 100 mM. It is observed that k_d and α values were greatest at 10 °C as compared to other temperatures ($P < 0.05$). Within this range of IS (3–100 mM), the k_d values at 10 °C varied from 7.1×10^{-4} to 1.4×10^{-2} s^{-1}, and α from 0.04 to 0.71. The k_d values varied from 4.5×10^{-4} to 1.4×10^{-2} s^{-1} at 4 °C, and 3.8×10^{-4} to 1.4×10^{-2} s^{-1} at 25 °C. The corresponding α values ranged from 0.02 to 0.6 and from 0.02 to 0.7 for 4 and 25 °C, respectively.

Column experiments using colloids were performed and resulting k_d and α values are presented in Fig. 5 and Table 3, respectively. The average k_d value for colloids at 25 °C was approximately three times greater than those at lower temperatures (1.5×10^{-3} s^{-1} at 25 °C versus 5.4×10^{-4} s^{-1} at 4 and 10 °C). Similarly, colloidal α was greatest at 25 °C with $\alpha = 0.08$ versus 0.03 at 4 and 10 °C (Table 3). It is observed that at high temperature (25 °C) colloidal k_d and α values were greater than those of bacteria but at lower temperatures the opposite is observed.

From the characterization experiments, it was observed that colloids were more hydrophobic than D21g. If hydrophobic interactions dominate interactions, it would be expected that colloidal k_d values would be greater than D21g, yet this is not so. This suggests hydrophobic interactions alone cannot explain observed deposition trends; rather deposition is likely due to the nature of colloidal and bacterial surfaces changing with temperature.

According to theory, α values should decrease with temperature, due to the expansion of the diffuse double layer thickness [20] and increased zeta potential (Tables 1 and 3); however, results suggest an additional phenomenon is involved. To determine whether mass transfer is responsible for the observed trends, deposition and collector efficiency was compared using filtration theory [33]. As shown in Tables 1 and 3, η_0 values calculated for colloids and bacteria increase with temperature due to the contributions of diffusion and sedimentation via decreasing fluid viscosity and density [33]. Under electrostatically favorable conditions deposition is controlled by the transport of particles to the collectors; therefore, the increasing η_0 values with temperature suggest $k_{d,fav}$ values should increase as well. However, the $k_{d,fav}$ trends for D21g and colloids are not consistent with this prediction. Overall, the $k_{d,fav}$ values for D21g and colloids were quite similar except for 4 °C at which D21g had greater transfer rate to the quartz surfaces than colloids ($P < 0.05$). Results indicate that D21g had the greatest $k_{d,fav}$ value at 4 °C (2.3×10^{-2} s^{-1}) ($P < 0.05$ compared to the values at other temperatures), while $k_{d,fav}$ values of colloids were virtually identical regardless of temperature (1.8×10^{-2}, 1.9×10^{-2}, and 1.9×10^{-2} s^{-1} for 4, 10, and 25 °C, respectively). It was also observed that there was no significant difference between D21g $k_{d,fav}$ values at 10 °C (2.0×10^{-2} s^{-1}) and 25 °C (2.0×10^{-2} s^{-1}). These results suggest the mass transfer is not changing significantly with temperature, and that observed variations in bacterial deposition can be attributed to a biological, rather than transport phenomenon.

Although deposition rates for colloids under unfavorable conditions (k_d) were highest at 25 °C, the overall percent increase with temperature was inconsistent with the predicted change in the collector efficiency, η_0. This also indicates transport is insufficient to explain the notably observed sensitivity to temperature. Colloidal η_0 and k_d values at 25 °C were 33 and 173% greater than those at 10 °C, respectively. Also, η_0 and k_d between 4 and 25 °C were found to increase 49 and 174%, respectively.

Table 3
Transport and surface characteristics of CML particles as a function of temperature. All experiments were conducted at 10 mM IS.

Temperature (°C)	MATH (%)[a]	Zeta potential (mV)	$k_{d,fav}$ (s^{-1})	η_0 (−)[b]	α (−)
4	95.3 ± 0.9	−73.8 ± 2.8	$1.8 \times 10^{-2} \pm 1.5 \times 10^{-3}$	2.6×10^{-3}	$3.1 \times 10^{-2} \pm 1.4 \times 10^{-4}$
10	95.7 ± 0.5	−76.6 ± 3.1	$1.9 \times 10^{-2} \pm 1.4 \times 10^{-3}$	3.0×10^{-3}	$2.8 \times 10^{-2} \pm 4.5 \times 10^{-4}$
25	94.4 ± 1.6	−84.8 ± 4.2	$1.9 \times 10^{-2} \pm 1.1 \times 10^{-3}$	3.9×10^{-3}	$7.8 \times 10^{-2} \pm 3.4 \times 10^{-3}$

[a] Microbial adhesion to hydrocarbon (MATH) indicates the relative hydrophobicity of the CML particles as the percent of particles partitioned in dodecane versus electrolyte (10 mM KCl).

[b] Calculated based upon Tufenkji and Elimelech [33].

Comparison of experimental results and traditional theory implies removal and interaction mechanisms not incorporated in the classic model [19] may be occurring. The filtration model was developed with the assumption that collectors are homogeneous and spherical [45], yet the quartz grains used in this study are irregularly and non-uniformly shaped [32]. Therefore, the difference between the model prediction and experimental data may also be attributed to the complicated pore structure [46,47], grain-grain contacts [48,49], and surface roughness [32,50]. The structural integrity of particles must also be considered. Cellular membrane fluidity [51] and latex elasticity are additional characteristics which vary with temperature and may explain deposition trends. Increased elasticity at greater temperature [52,53] may contribute to the high k_d and α values at 25 °C.

Another possible particle characteristic leading to the observed trends is surface chemistry. Temperature enhances colloid hydrophobicity, resulting from conformational changes of carboxyl groups on outer surface [54]. Similar to colloids, D21g surface chemistry and deposition trends were sensitive to temperature; however, unlike colloids α was greatest at 10 °C, indicating the occurrence of an additional biological factor. Table 2 shows EPS variation with temperature, for cells prepared in the identical procedure as those utilized in transport experiments; however, this data cannot explain the deposition behavior of D21g at 10 °C. Previous studies have observed cell properties changing with temperature [55,56]; however the distinct behavior at 10 °C is novel. It is hypothesized that at 10 °C cells are at a particular metabolic and physiological state such that other physiological characteristics not measured in this study (i.e., membrane fluidity [51], surface hydrophobicity [57], or polymer conformation [58]) may be involved.

4. Conclusions

Average k_d and α values for D21g in the presence of KCl and $CaCl_2$ are presented as a function of IS at different temperatures in Figs. 3 and 4, respectively. Based upon zeta potential data, it is suggested at low to moderate IS the deposition results are primarily attributed to electrostatic repulsion. This is evident by the sensitivity of D21g deposition to IS and the extent of deposition in $CaCl_2$ being greater than in KCl solution at all IS and temperatures. However, at IS > 100 mM (i.e., electrostatically favorable region) [23,39] α for cells in $CaCl_2$ are even greater than unity at 10 and 25 °C, suggesting an additional, non-electrostatic mechanism is involved.

Although sensitive to IS, in the presence of Ca^{2+} deposition appears insensitive to temperature. Additional evidence is found through consideration of the favorable experiments conducted in the presence of Ca^{2+}, when cells were less negative than those in KCl and electrostatic interactions should result in less attachment to the positively charged silanized surface. However, $k_{d,fav}$ values were slightly greater than those in KCl solution at all temperatures. This is likely due to the Ca^{2+} influencing cell surface polymers interaction with the silanized surface – which occurs regardless of the temperature – likely occurring via charge neutralization or altering polymer conformation [6,16,40]. Ca^{2+} may alter the extent and distribution of polar functional groups, and enhance the degree of cell surface charge heterogeneity at a local level, ultimately impacting the extent of electrostatic interactions [6,59]. This is similar to observations for unfavorable conditions, in that the presence of Ca^{2+} ions – regardless of temperature – contributes to non-specific interactions, as supported by DCB theory [42,43] and influences the extent of deposition.

Acknowledgements

This research was funded in part by the National Water Research Institute (05-WQ-005) and the USDA CSREES NRI (2006-02541). The authors express their gratitude to Shiva ShojaeTazehkand, Crystal Bray, and Matthew Yates for their assistance in the reported experiments.

References

[1] M.L. Rockhold, R.R. Yarwood, J.S. Selker, Vadose Zone J. 3 (2004) 368.
[2] T.K. Stevik, K. Aa, A. Geir, J.F. Hanssen, Water Res. 38 (2004) 1355.
[3] S.A. Bradford, J. Simunek, S.L. Walker, Water Resour. Res 42 (2006) W12S12, doi:10.1029/2005WR004805.
[4] D.R. McCaulou, R.C. Bales, R.G. Arnold, Water Resour. Res. 31 (1995) 271.
[5] M.J. Hendry, J.R. Lawrence, P. Maloszewski, Ground Water 37 (1999) 103.
[6] G. Chen, S.L. Walker, Langmuir 23 (2007) 7162.
[7] N. Yee, J.B. Fein, C.J. Daughney, Geochim. Cosmochim. Acta 64 (2000) 609.
[8] H. Dong, R. Rothmel, T.C. Onstott, M.E. Fuller, M.F. DeFlaun, S.H. Streger, R. Dunlap, M. Fletcher, Appl. Environ. Microbiol. 68 (2002) 2120.
[9] A. Schafer, P. Ustohal, H. Harms, F. Stauffer, T. Dracos, A.J.B. Zehnder, J. Contam. Hydrol. 33 (1998) 149.
[10] H. Dong, J. Microbiol. Methods 50 (2002) 83.
[11] T.A. Camesano, B.E. Logan, Environ. Sci. Technol. 32 (1998) 1699.
[12] D.E. Fontes, A.L. Mills, G.M. Hornberger, J.S. Herman, Appl. Environ. Microbiol. 57 (1991) 2473.
[13] H. Dong, T.C. Onstott, M.F. DeFlaun, M.E. Fuller, T.D. Scheibe, S.H. Streger, R.K. Rothmel, B.J. Mailloux, Environ. Sci. Technol. 36 (2002) 891.
[14] N.I. Abu-Lail, T.A. Camesano, Environ. Sci. Technol. 37 (2003) 2173.
[15] S. Tsuneda, H. Aikawa, H. Hayashi, A. Yuasa, A. Hirata, FEMS Microbiol. Lett. 223 (2003) 287.
[16] Z.A. Kuznar, M. Elimelech, Environ. Sci. Technol. 38 (2004) 6839.
[17] H.-H. Yang, The effect of environmental stress on cell surface properties and their relation to microbial adhesion in feedlot *Escherichia coli* isolates, Doctoral Dissertation, University of Connecticut, Storrs, CT, 2005.
[18] F.D. Castro, N. Tufenkji, Environ. Sci. Technol. 41 (2007) 4332.
[19] K.-M. Yao, M.T. Habibian, C.R. O'Melia, Environ. Sci. Technol. 5 (1971) 1105.
[20] M. Elimelech, J. Gregory, X. Jia, R.A. Williams, Particle Deposition and Aggregation: Measurement, Modeling and Simulation, Butterworth-Heinemann, Oxford, England, 1995.
[21] B.D. Horne, E.S. Rutherford, K.E. Wehrly, River Res. Appl. 20 (2004) 185.
[22] V.F. Bense, H. Kooi, J. Geophys. Res. 109 (2004) B04103, doi:04110.01029/02003JB002782.
[23] J.A. Redman, S.L. Walker, M. Elimelech, Environ. Sci. Technol. 38 (2004) 1777.
[24] W. Lee, T.K. Wood, W. Chen, Biotechnol. Bioeng. 95 (2006) 399.
[25] M.J. Martin, B.E. Logan, W.P. Johnson, D.G. Jewett, R.G. Arnold, J. Environ. Eng. 122 (1996) 407.
[26] R.S. Pembrey, K.C. Marshall, R.P. Schneider, Appl. Environ. Microbiol. 65 (1999) 2877.
[27] Y. Shim, H.J. Lee, S. Lee, S.H. Moon, J. Cho, Environ. Sci. Technol. 36 (2002) 3864.
[28] R. Switzer, L. Garrity, Environmental Biochemistry, W.H. Freeman Publishing, 1999.
[29] M. DuBois, K.A. Gilles, J.K. Hamilton, P.A. Rebers, F. Smith, Anal. Chem. 28 (1956) 350.
[30] Z. Adamczyk, B. Siwek, M. Zembala, P. Warszynski, J. Colloid Interface Sci. 130 (1989) 578.
[31] R. Kretzschmar, M. Borkovec, D. Grolimund, M. Elimelech, Adv. Agron. 66 (1999) 121.
[32] N. Tufenkji, G.F. Miller, J.N. Ryan, R.W. Harvey, M. Elimelech, Environ. Sci. Technol. 38 (2004) 5932.
[33] N. Tufenkji, M. Elimelech, Environ. Sci. Technol. 38 (2004) 529.
[34] M. Elimelech, C.R. O'Melia, Colloids Surf. 44 (1990) 165.
[35] B.V. Derjaguin, L.D. Landau, Acta Physicochim. 14 (1941) 733.
[36] S.L. Walker, J.A. Redman, M. Elimelech, Environ. Sci. Technol. 39 (2005) 6405.
[37] A. Razatos, Y.-L. Ong, M.M. Sharma, G. Georgiou, Proc. Natl. Acad. Sci. 95 (1998) 11059.
[38] K. Otto, M. Hermansson, J. Bacteriol. 186 (2004) 226.
[39] K.L. Chen, S.E. Mylon, M. Elimelech, Environ. Sci. Technol. 40 (2006) 1516.
[40] W. Khemakhem, E. Ammar, A. Bakhrouf, World J. Microbiol. Biotechnol. 21 (2005) 1623.
[41] A. Zita, M. Hermansson, Appl. Environ. Microbiol. 63 (1997) 1168.
[42] R.E. McKinney, Sewage Ind. Wastes 24 (1952) 280.
[43] Y. Tezuka, Appl. Environ. Microbiol. 17 (1969) 222.
[44] Q. Li, M. Elimelech, Environ. Sci. Technol. 38 (2004) 4683.
[45] J. Happel, AIChE J. 4 (1958) 197.
[46] S.A. Bradford, S.R. Yates, M. Bettahar, J. Simunek, Water Resour. Res. 38 (2002) 1327.
[47] S.A. Bradford, M. Bettahar, J. Simunek, M.T. van Genuchten, Vadose Zone J. 3 (2004) 384.
[48] S.A. Bradford, S. Torkzaban, S.L. Walker, Water Res. 41 (2007) 3012.
[49] W.P. Johnson, X. Li, G. Yal, Environ. Sci. Technol. 41 (2007) 1279.
[50] M. Auset, A.A. Keller, Water Resour. Res. 42 (2006) W12S02.

[51] R. Tourdot-Marechal, D. Gaboriau, L. Beney, C. Divies, Int. J. Food Microbiol. 55 (2000) 269.
[52] J.F. Rudd, E.F. Gurnee, J. Appl. Phys. 28 (1957) 1096.
[53] V.V. Bagreev, Mech. Compos. Mater. 10 (1974) 1122.
[54] H. Guo, D. Liang, S. Ramakrishnan, C.F. Zukoski, J.L. Harden, R.L. Leheny, Evolution of particle-scale dynamics in suspensions of weekly attractive colloids undergoing structural arrest, in: The MAR06 Meeting of the American Physical Society, 2006.
[55] R.E. Sjogren, Water Air Soil Pollut. 75 (1994) 389.
[56] J.W.A. Foppen, J.F. Schijven, Water Res. 40 (2006) 401.
[57] A.M. Gallardo-Moreno, M.L. Gonzalez-Martin, J.M. Bruque, C. Perez-Giraldo, R. Sanchez-Silos, A.C. Gomez-Garcia, J. Adhes. Sci. Technol. 17 (2003) 1877.
[58] T. Drobek, N.D. Spencer, M. Heuberger, Compressing PEG brushes, Macromolecules 38 (2005) 5254.
[59] A.J. deKerchove, M. Elimelech, Biomacromolecules 8 (2007) 113.